PNAS Nexus, 2024, 3, pgae528
https://doi.org/10.1093/pnasnexus/pgae528
Advance access publication 21 November 2024
Research Report

Cryo-EM structure of histidyl-tRNA synthetase-like domain reveals activating crossed helices at the core of GCN2

Kristina Solorio-Kirpichyan[a], Xiao Fan[a,b,1,2], Dmitrij Golovenko[c,2], Andrei A. Korostelev[c], Nieng Yan[a,b] and Alexei Korennykh[a,*]

[a]Department of Molecular Biology, Princeton University, Princeton, NJ 08544, USA
[b]Shenzhen Medical Academy of Research and Translation, Shenzhen, Guangdong 518107, China
[c]RNA Therapeutics Institute, University of Massachusetts Chan Medical School, 368 Plantation Street, Worcester, MA 01605, USA
*To whom correspondence should be addressed: Email: akorenny@princeton.edu
[1]Present address: Laboratory of Neurophysiology and Behavior, The Rockefeller University, New York, NY, USA
[2]X.F. and D.G. contributed equally to this work.
Edited By Cheng Zhang

Abstract

GCN2 is a conserved receptor kinase activating the integrated stress response (ISR) in eukaryotic cells. The ISR kinases detect accumulation of stress molecules and reprogram translation from basal tasks to preferred production of cytoprotective proteins. GCN2 stands out evolutionarily among all protein kinases due to the presence of a histidyl-tRNA synthetase-like (HRSL) domain, which arises only in GCN2 and is located next to the kinase domain (KD). How HRSL contributes to GCN2 signaling remains unknown. Here, we report a 3.2 Å cryo-EM structure of HRSL from thermotolerant yeast *Kluyveromyces marxianus*. This structure shows a constitutive symmetrical homodimer featuring a compact helical-bundle structure at the junction between HRSL and KDs, in the core of the receptor. Mutagenesis demonstrates that this junction structure activates GCN2 and indicates that our cryo-EM structure captures the active signaling state of HRSL. Based on these results, we put forward a GCN2 regulation mechanism, where HRSL drives the formation of activated kinase dimers. The remaining domains of GCN2 have the opposite role and in the absence of stress they help keep GCN2 basally inactive. This auto-inhibitory activity is relieved upon stress ligand binding. We propose that the opposing action of HRSL and additional GCN2 domains thus yields a regulated ISR receptor.

Keywords: GCN2, structure, cryo-EM, integrated stress response

Significance Statement

Regulation of protein synthesis (translation) is a central mechanism by which eukaryotic cells adapt to stressful conditions. In starving cells, this translational adaptation is achieved via the receptor kinase GCN2, which stays inactive under normal conditions, but is switched on under stress. The molecular mechanism of GCN2 switching is not well understood due to the presence of a structurally and biochemically uncharacterized histidyl-tRNA synthetase-like domain (HRSL) at the core of GCN2. Here, we use single-particle cryo-EM and biochemistry to elucidate the structure and function of HRSL. We identify a structure at the kinase/HRSL interface, which forms crossed helices and helps position GCN2 kinase domains for activation. These data clarify the molecular mechanism of GCN2 regulation.

Introduction

GCN2 is a stress kinase from the family of four translation initiation factor 2α (eIF2α) kinases (1, 2). These kinases sense signaling molecules produced specifically in stressed cells and phosphorylate a regulatory serine residue of translation initiation factor eIF2α. Phosphorylation of eIF2α inhibits the initiation step of protein synthesis and activates the integrated stress response (ISR) to allow cell adaptation to stress. The ISR attempts to reestablish normal cell function by reprogramming gene expression, and if homeostasis cannot be achieved, the ISR activates apoptosis (2).

The four ISR receptor kinases are GCN2, HRI, PERK, and PKR. They contain homologous kinase domains (KDs), which recognize and phosphorylate eIF2α. The KDs are linked to different stress-sensing and regulatory domains for each family member. These domains allow GCN2 to sense the nutrient status of a cell (2, 3), HRI to sense heme (4), PERK to sense unfolded proteins (5), and PKR to sense

Competing Interest: The authors declare no competing interests.
Received: October 8, 2024. **Accepted:** November 13, 2024

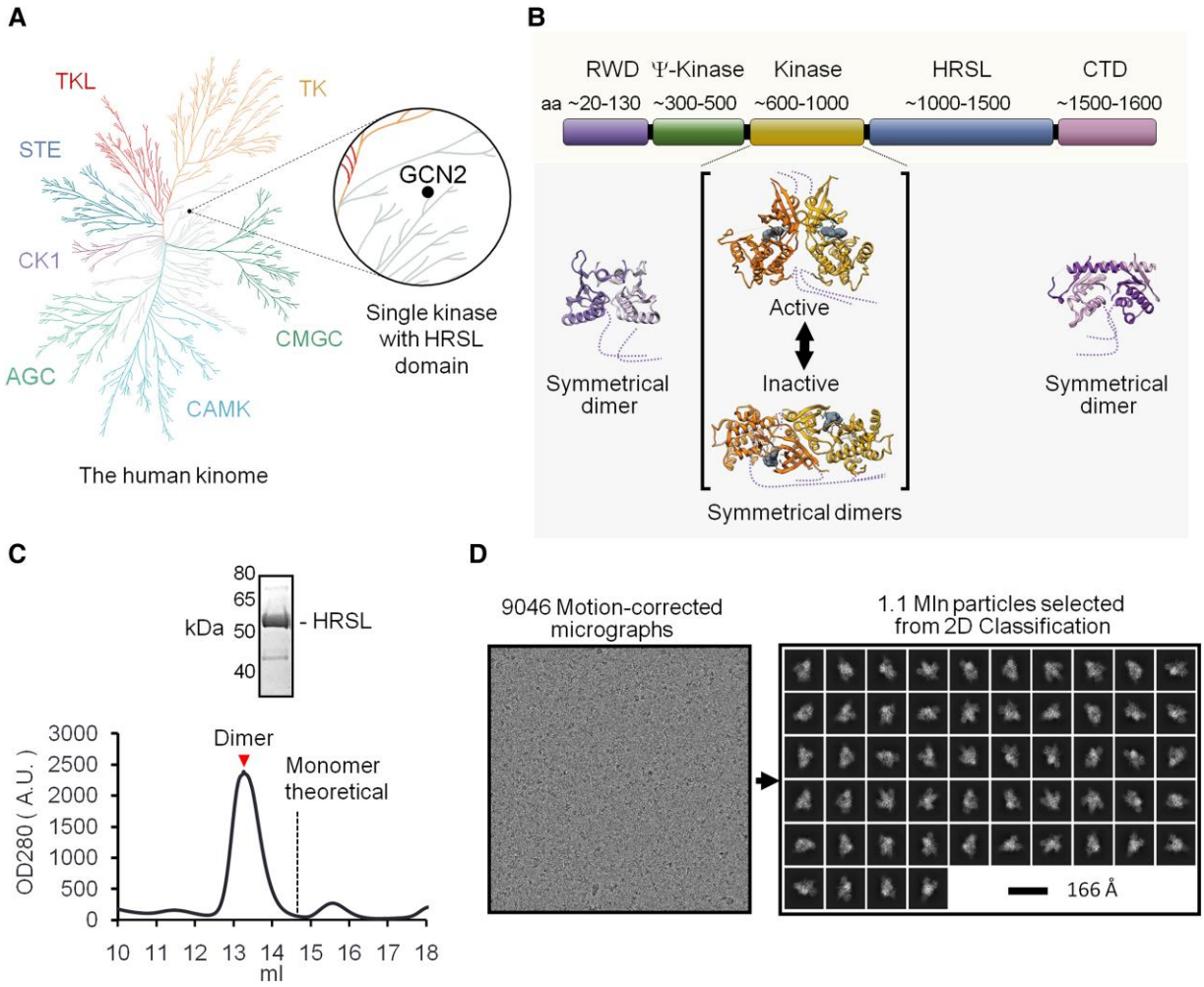

Fig. 1. Phylogenetic attributes of GCN2 and characterization of HRSL domain. A) Location of GCN2 within human kinome. B) Domain architecture of GCN2 with available crystal structures superimposed. PDB codes of shown structure: RWD 7E2M; kinase 6N3O (active dimer) 1ZYD (inactive dimer); CTD 4OTM. C) Left: Size exclusion chromatography FPLC trace of purified GCN2 HRSL. GCN2 HRSL runs at a molecular weight consistent with a dimer at ~120 kDa. Right: Coomassie-stained SDS–PAGE with purified GCN2 HRSL collected from indicated fraction (marker). D) Left: Representative motion-corrected cryo-EM micrograph for GCN2 HRSL. Right: Classes selected from final round of 2D classification used for initial 3D reconstruction.

harmful double-stranded RNA (6, 7). GCN2$^{-/-}$ mice have few pups under low-leucine diet and develop severe liver steatosis when under amino acid deprivation due to importance of GCN2 in metabolic regulation of nutrients (8, 9). Depending on the type of training, GCN2$^{-/-}$ mice can exhibit enhanced or impaired learning ability, supporting the broad role of the ISR in cognitive processes (2, 10, 11).

Structural and biochemical studies have shown that regulation of the ISR kinases uses homo-dimerization, although the precise mechanisms of dimerization coupling to the ligand-sensing domains remain poorly understood for all ISR kinases (6). Structures of every major domain are available for two of the four receptors: PERK and PKR. These structures with biochemical and other studies provide perhaps the most complete models of regulation among ISR kinases (5–7, 12–14). GCN2 is the largest ISR receptor kinase featuring five globular domains. Structures of three GCN2 domains have been reported. At the N terminus, GCN2 contains the Ring finger-WD repeat-DEAD-like helicase domain (RWD), which forms a stable homodimer and binds to GCN2 partner proteins GCN1/GCN20 (15–17) (Fig. 1B, PDB ID 7E2M). At the C terminus, GCN2 contains the C-terminal domain (CTD), which also forms a homodimer and apparently has two functions: binding to the ribosome and auto-inhibition of the kinase (18, 19) (Fig. 1B, PDB 4OTM). Finally, structures of the KD have been determined for two functionally relevant dimeric states. They revealed a head-to-head inactive dimer (20) (Fig. 1B, PDB 1ZYD) and a back-to-back active dimer, which is similar to active dimers formed by other protein kinases (21, 22) (Fig. 1B, PDB 6N3O and 7QQ6). Structure of GCN2 pseudo-kinase domain (ΨKD), proposed to help GCN2 activation (23), remains unknown. The largest GCN2 domain, sharing 22% sequence identity with histidyl-tRNA synthetase HisRS (HisRS-like domain, HRSL; Fig. 1A and B), has remained structurally uncharacterized until recently.

The deficit of structural information about major domains of GCN2 and the absence of tRNA synthetase-like domains in other, better-studied protein kinases (Fig. 1A) (24) limits our understanding of the molecular mechanism of GCN2. To lift this limitation, here we present single-particle cryo-EM and biochemical analyses of GCN2 HRSL, offering insights into the function of HRSL.

Results

Cryo-EM structure of GCN2 HRSL domain reveals an intertwined homodimer

To characterize the HRSL domain, we cloned GCN2 from three species—human, *S. cerevisiae*, and thermotolerant yeast

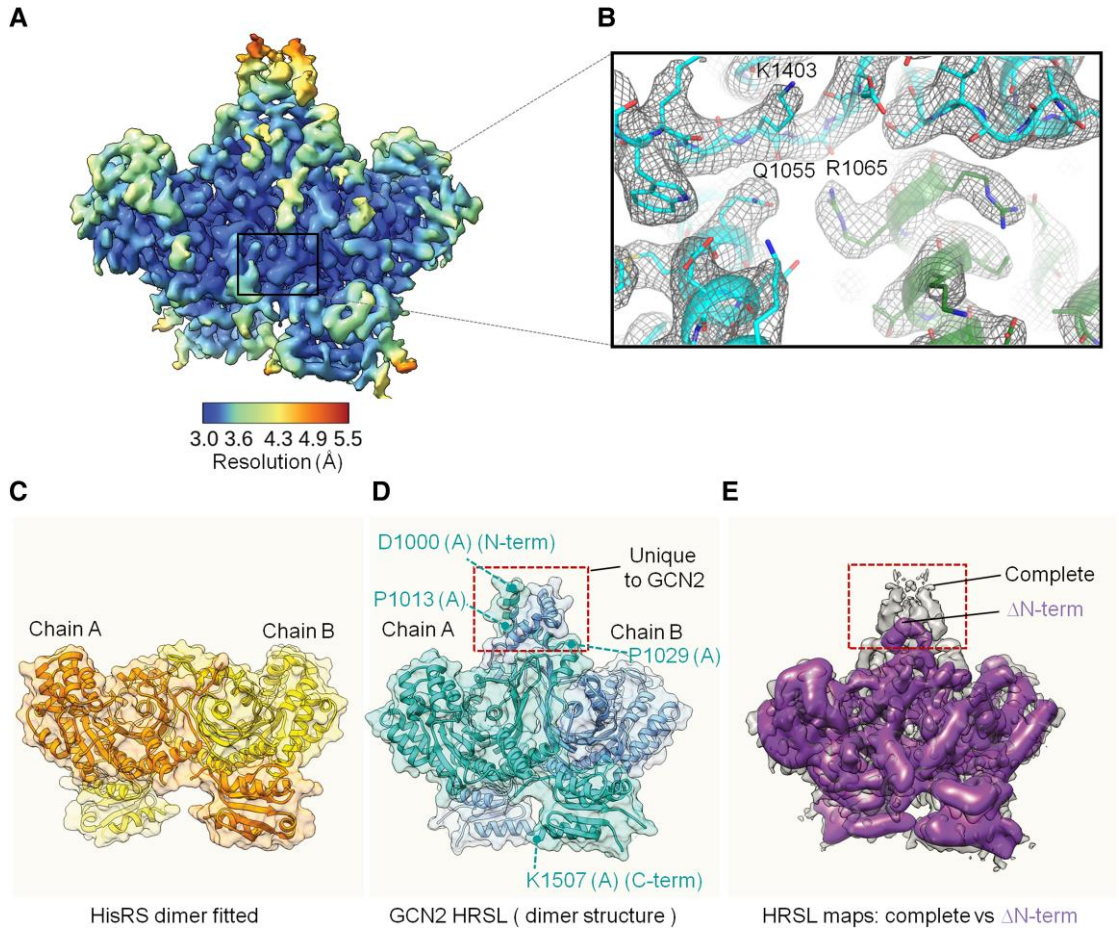

Fig. 2. Cryo-EM structure analysis of GCN2 HRSL domain. A) Final sharpened GCN2 HRSL cryo-EM map generated from CryoSPARC, surface colored by local resolution based on gold-standard FSC threshold 0.143. B) Representative densities of amino acid backbone and side chains. C) Structure tRNA synthetase HisRS (PDB ID 4RDX). D) Structure of GCN2 HRSL. Boxed region shows a unique subdomain absent in HisRS. E) Cryo-EM map for ΔN-terminal GCN2 HRSL dimer (purple) superimposed onto the cryo-EM map of GCN2 HRSL (gray) (Tables S1 and S2).

Kluyveromyces marxianus—and subsequently purified the corresponding HRSL domains, both individually and with flanking domains of various length. *Kluyveromyces* sequence yielded a soluble homogeneous HRSL domain suitable for structural studies (residues 996–1,511; Materials and methods). HRSL migrated as a stable homodimer (Fig. 1C). Milligram quantities of *Kluyveromyces* HRSL were produced and tested in high-throughput crystallization screens, without success. By contrast, well-dispersed Quantifoil Cu grid samples suitable for cryo-EM analysis were successfully prepared (Fig. 1D).

We determined a 3.2 Å cryo-EM structure of GCN2 HRSL (Fig. S1; Table S1), in which most side chains are well resolved (Fig. 2A and B). To build the structure of GCN2 HRSL, we generated an initial AlphaFold model from protein sequence (25) (Materials and methods). The predicted model, containing a crossed homodimer formed by intertwined monomers, had a nearly perfect fit into the map and required only minor corrections of several side chains and a conservative all-atom refinement to achieve the final structure (Fig. 2A–D; Materials and methods). Compared with HRSL HisRS (26), GCN2 HRSL has an additional N-terminal structure comprised of bundled alpha-helices (Fig. 2C and D, boxed). Truncation of these N-terminal helices in a mutant Δ(V996-N1009) caused a loss of the N-terminal density, providing experimental verification of correct helix placement in our model (Figs. 2E and S2A–C; Table S2). Concomitantly with our work, a related study described 3.2A cryo-EM stricture of human HRSL was published (27), revealing structural conservation of HRSL from yeasts to humans.

Conservation analysis of HRSL surface electrostatics suggests a loss of tRNA complementarity

Based on sequence homology with His-tRNA synthetase HisRS, HRSL domain of GCN2 was initially proposed to also bind free tRNAs, modestly preferring deacylated tRNAs, to sense the nutritional status of a cell (28). An alternative and perhaps complementary recent model proposes that GCN2 binds the P-stalks of stalled ribosomes, using the ribosome to sense whether the cell undergoes a translational stress (29–31). The HRSL domain is linked directly to the KD, and thus, it should play a role in regulation. Indeed, strong activation of GCN2 kinase by ribosomes depends on HRSL (30).

Here, we assessed the phylogenetic–structural conservation of the electrostatic potential to evaluate the tRNA-sensing model. We analyzed and compared the conserved tRNA interaction site of HisRS with the equivalent surface of HRSL of GCN2 proteins by computing conserved electrostatic potentials (Materials and methods). Our analysis takes into account 3D structures and evolutionary conservation of amino acid charges obtained from

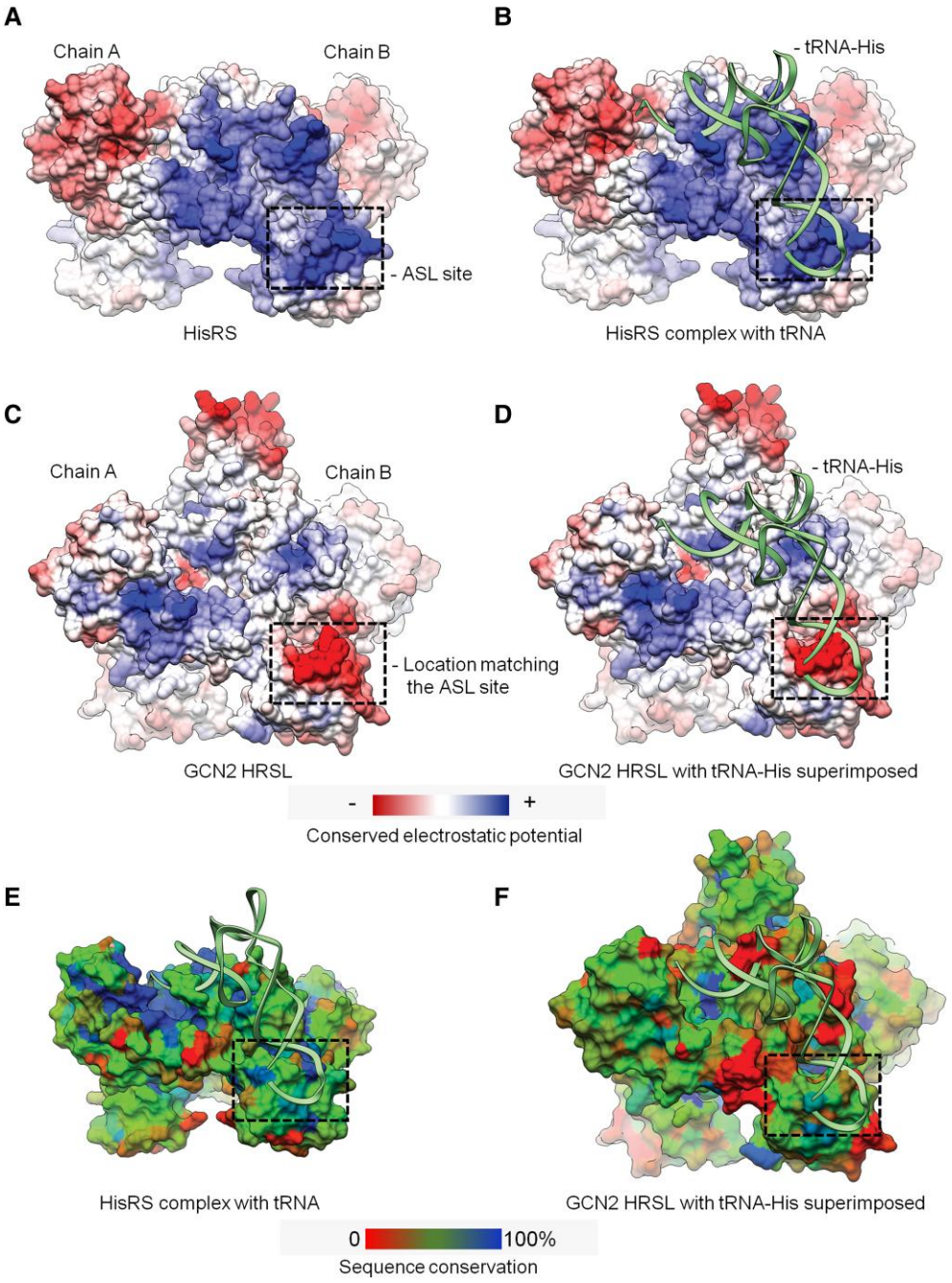

Fig. 3. Comparison of conservation in tRNA synthetase HisRS vs. GCN2 HRSL. A) HisRS structure (PDB: 4RDX) colored by the conserved electrostatic potential (Materials and methods). Dotted box indicates ASL site. Bound tRNA is hidden for visualization of surface charge. B) Structure from (A) with bound tRNA (green). C) GCN2 HRSL structure colored by the conserved electrostatic potential. D) Structure from (C) with tRNA (green) docked to the surface of HRSL domain based on structure alignment with HisRS (B). E) HRS colored by protein sequence conservation using BLOSUM62 matrix (Materials and methods). F) HRSL colored by protein sequence conservation using BLOSUM62 matrix as in (E).

multiple sequence alignments of more than 190 eukaryotic proteins, from yeasts to human. HisRS exhibits an evolutionarily conserved positive surface potential that tracks well with tRNA (Fig. 3A and B), as expected for the recognition of the negatively charged tRNA backbone. By contrast, HRSL of GCN2 lacks the electrostatic complementarity with tRNA and harbors a conserved antagonizing negatively charged patch at the putative binding site for tRNA anticodon stem-loop (ASL) (Fig. 3C and D). The remaining weaker positive charge at the putative acceptor arm binding site (Fig. 3C and D) may underlie the detectable affinity toward tRNA, as considered in Discussion below.

Our conclusions derived from conserved electrostatics are in line also with standard protein conservation analysis. The surface of HRSL shows worse match with tRNA, including the catalytic center and the area of ASL interaction (Fig. 3E vs. F).

HRSL connects to the KD via dimerized junction α-helices

The N-terminal part of HRSL (aa 1,000–1,029) contains two sequential α-helices, which are absent in tRNA synthetases and form a symmetrical parallel homodimer (bundle) in the dimeric

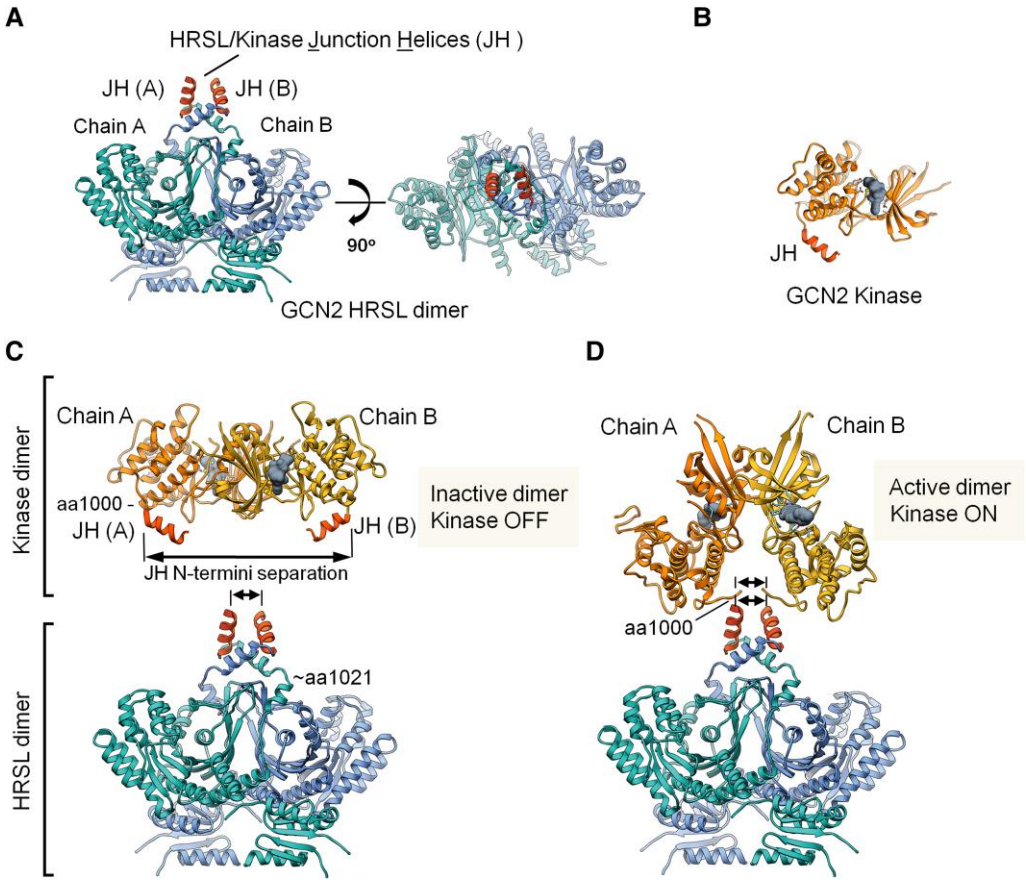

Fig. 4. Dimerized α-helices JH connect HRSL and KDs. A) GCN2 HRSL dimer with junction helices (JH) colored red for each chain. B) GCN2 KD (monomer-PDB: 1ZYD) with JH colored red. C–D) Structure of inactive (PDB: 1ZYD) and active (PDB: 6N3O) dimers of GCN2 KD next to the dimer of GCN2 HRSL. Distances between equivalent amino acids in kinase and HRSL domains are marked with arrows. The inactive dimer has the KDs bound N-lobe-to-N-lobe, with anchor points for JH helices well separated. The KDs adapt the inactive (α-C helix-out) conformation. The active dimer has the KDs bound back-to-back, with anchor point for JH helices positioned proximally. The KDs adapt the active (α-C helix-in) conformation. Amino acid numbers (aa) match numbers in *K. marxianus*.

HRSL structure (Figs. 2B–D and 4A). The bundle is kept by extensive hydrophobic interactions. Helix 1 of one HRSL copy (D1000-P1013, Fig. 2D) is followed by helix 2 (S1014-P1029) placed at an angle. Two symmetry-related helices from the partner chain complete the bundle. The core is held by I1003, L1007, and I1010 (helix 1) and W1017, V1021, and L1025 (helix 2) from both HRSL monomers. The first helix has been captured in the previous crystal structure of GCN2 KD; however, its role could not be assigned: neither does it pack compactly with the rest of the kinase nor is it located proximally to known functional sites of kinase (20) (Fig. 4B). Our work now shows that the α-helix is a part of HRSL domain, serving as kinase/HRSL junction helix (JH).

Analogous to the HRSL domain, which exists as a stable homodimer, the KD of GCN2 also forms a homodimer. Structural studies identified two types of dimers for GCN2 kinase. The first type contains the catalytically inactive "OFF" conformation of kinase (PDB ID 1ZYD) (20), whereas the second type contains the catalytically active "ON" conformation of kinase (PDB ID 6N3O) (21). To understand how HRSL could interact with these dimers, we placed either dimeric kinase next to the dimeric HRSL from our cryo-EM structure. The dimer of GCN2 kinases in the "OFF" state is sterically incompatible with our structure due to the large distance between the N termini of JH in kinase compared with that in HRSL dimer (Fig. 4C). In contrast, structure of the dimeric kinase in "ON" conformation matched well with the HRSL dimer (Fig. 4C and D). The cryo-EM structure of HRSL therefore likely represents the active signaling state of GCN2.

JH dimerization activates GCN2

Dimerization of JH helices at the core of GCN2 suggests their role in regulating the receptor, whereas the steric match with the active kinase dimer (Fig. 4) indicates that JH/JH interaction activates (rather than inhibits) the kinase output. To test this hypothesis, we developed an assay for quantitative biochemical analysis of GCN2 kinase activity based on a previous publication (29). We measured phosphorylation of eIF2α by the GCN2 construct comprising the N-terminally FLAG-tagged kinase/HRSL domains of thermotolerant yeast (residues 578–1,511; Table S2) purified from HEK293 cells (Materials and methods). As a control for nonspecific interactions with antiflag resin, we used a mock pulldown from naïve HEK293 cells.

Time-dependent phosphorylation of eIF2α was observed in the presence of GCN2 kinase/HRSL (Fig. S3A–C; Table S3). Eluates from naïve pulldowns did not cause eIF2α phosphorylation, indicating that the observed kinase activity arises specifically from the transfected GCN2 construct rather than from a stray cellular kinase activity (Fig. S3). To test whether GCN2 kinase/HRSL construct is truly active autonomously or might depend on an accidentally co-purified cellular RNA, we treated GCN2 kinase/HRSL with an excessive (300 nM) concentration of RNase A. RNase

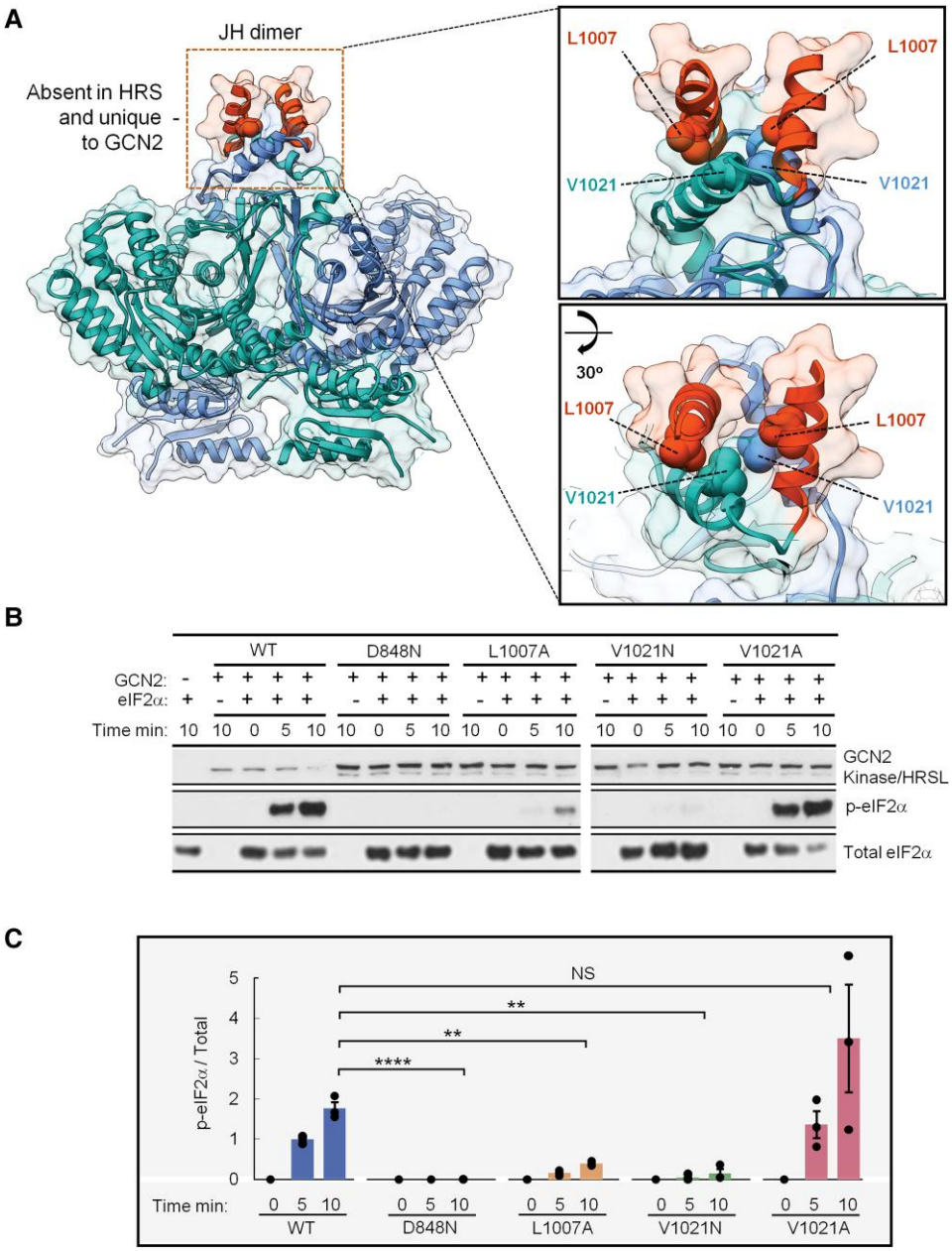

Fig. 5. Close-up view of JH/JH interface and functional analysis of GCN2 activation. A) Structure of HRSL with JH helices colored orange. The interface between dimerized helices JH is created by several closely packed hydrophobic side chains. We selected hydrophobic amino acid L1007 in JH and hydrophobic amino acid V1021 located in α-helix immediately downstream of JH for mutagenesis. The α-helix harboring V1021 together with JH contributes to the formation of the α-helical bundle present in GCN2 and absent in HisRS. Two rotationally related close-up views of the bundle structure are showed in boxed panels. B) In vitro kinase activity for WT and interface mutants (L1007A, V1021A, and V1021N) in GCN2 kinase/HRSL ("K/HRSL") visualized by western blot. C) Quantification of biochemical data for the mutants D848N, L1007A, V1021A, and V1021N. Statistical significance (P) was calculated using Welch's two-tailed unpaired t test: *P*-value ≤0.05*, ≤ 0.01**, ≤ 0.001***, ≤ 0.0001****, N.S: nonsignificant.

A treatment did not inhibit the eFI2α phosphorylation activity of GCN2 kinase/HRSL (Fig. S4). These results with GCN2 kinase/HRSL from thermotolerant yeast agree with those obtained using GCN2 kinase/HRSL from human, which also demonstrated constitutive catalytic activity in the absence of tRNAs and ribosomes (29).

We next tested whether disruption of the JH/JH helical homodimer affects the catalytic activity of GCN2. Due to unavailability of biochemically well-behaved full-length GCN2, we used the same kinase/HRSL construct as above. Therefore, we must note that our analysis relies on the expectation that functional interactions between HRSL and kinase in the kinase/HRSL construct are representative of those in the native receptor.

We tested mutations of hydrophobic residues L1007A, V1021N, and V1021A located at the core of the N-terminal helical bundle in our cryo-EM structure (Fig. 5A). As a positive control for activity readout with mutants, we tested a known catalytically dead mutant D848N (29), in which the nucleophilic aspartate required for proton transfer is replaced by noncatalytic isosteric asparagine (Fig. 5B and C; S5). The mutation L1007A was detrimental to activity of GCN2 kinase/HRSL, indicating that the amino acid L1007 forms a functional interaction that helps maintain GCN2 kinases

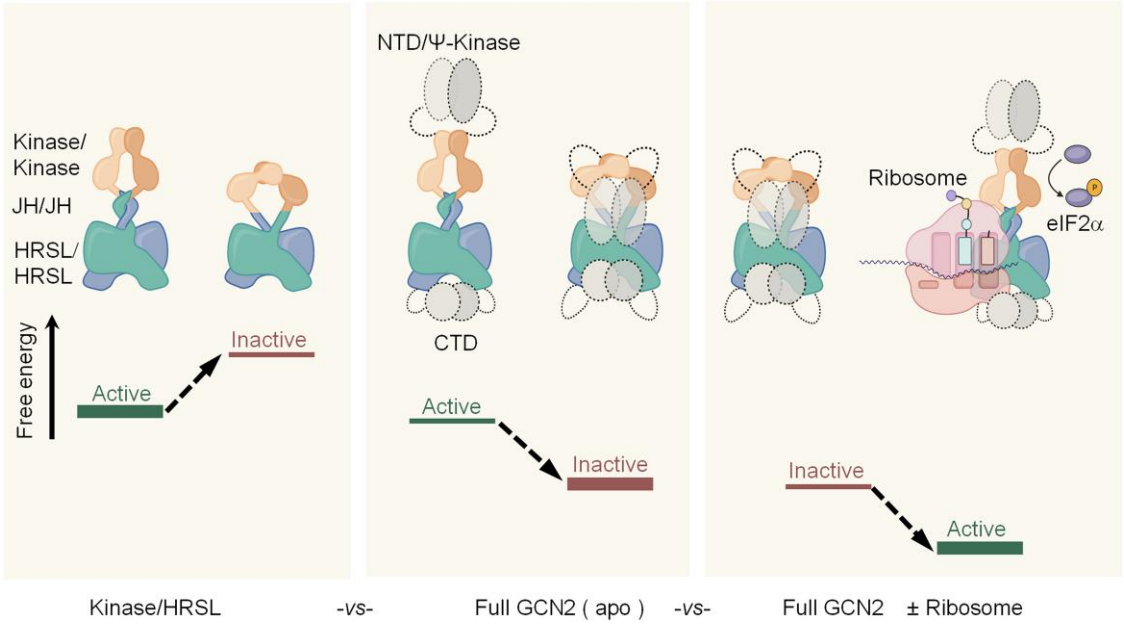

Fig. 6. Proposed model of GCN2 regulation. Relative free energies for kinase/HRSL (left panel), full-length GCN2 (middle panel), and GCN2 bound to the ribosome (right panel) are marked. Kinase/HRSL core of GCN2 favors active conformation, aided by JH/JH interface. Additional domains are auto-inhibitory, while ribosome binding releases the auto-inhibition.

in the active dimeric state. The mutation V1021A was neutral, indicating that although alanine is smaller than valine, it is sufficiently hydrophobic to preserve JH/JH interaction. In contrast, a more invasive mutation V1021N interfered sufficiently to disrupt the kinase activity (Figs. 5 and S5).

Discussion

Two features stand out in the structure of GCN2 HRSL domain: the loss of electrostatic complementarity to tRNA and the presence of a compact helical bundle formed via dimerization of α-helices JH connecting kinase and HRSL. The loss of the electrostatic complementarity, conserved from yeasts to human (Fig. 3), provides a biophysical argument against binding of free tRNAs to GCN2 HRSL as the main stress-sensing step and indicates that sensing stressed ribosomes via ribosomal P-stalk could be the primary mechanism (29–31). Indeed, the apparent K_d values of tRNA interaction with mammalian GCN2, estimated at ~2 μM (32) and ~4 μM in the recent study by Yin et al. (27), reflect a substantially weaker affinity than for tRNA binding by a mammalian histidyl-tRNA synthetase (K_m ~ 6 nM) (33). In line with this, 5 μM tRNA fails to activate GCN2 (29, 30), whereas nanomolar concentrations of the isolated ribosome or the isolated P-stalk are sufficient for GCN2 activation in vitro (29, 30). The P-stalk is required for GCN2 activation in most starved or otherwise stressed mammalian and yeast cells (30, 31, 34–36), in keeping with the stalled ribosome being the major activator of GCN2.

Additionally, a unified mechanism of GCN2 activation by both the P-stalk and tRNA may play a role. In this model, the loss of electrostatic complementarity to tRNA could be beneficial to desensitize GCN2 to specific tRNAs and render the receptor sensitive to all accessible acceptor arms in tRNAs that co-bind to the ribosome. This is consistent with the observation that under synthetic conditions, yeast GCN2 can be activated by amino acid deprivation in P-stalk-deficient strains, where deacylated tRNAs appear to be the primary activator presumably due to their accumulation to high levels in the absence of the timely stress response (31, 36).

The second major feature of HRSL, JH helix, plays a central role in regulation of GCN2. Dimeric HRSL with dimerized JH/JH region is structurally complementary only to the active configuration of dimeric GCN2 kinase (Fig. 4C vs. D). This conclusion is supported by biochemical analyses (Figs. 5B, C and S5) and confirms that our cryo-EM structure represents the kinase-activating state of HRSL. Based on these observations, we propose a mechanism of GCN2 regulation, which predicts free energy relationships and roles of multiple domains of this receptor. The thermodynamic role of HRSL is to favor the catalytically active dimers of GCN2 kinase (Fig. 6, first panel). If these additional domains were absent, GCN2 would exhibit uncontrollable, persistent activity with harmful consequences, such as apoptosis due to global translational arrest. Therefore, the free energy role of at least some of the additional domains of GCN2, present besides kinase and HRSL, is to counteract the action of HRSL and auto-inhibit the receptor under basal conditions (Fig. 6, middle panel). The previously proposed auto-inhibitory action of CTD is in line with this model (18, 19). The auto-inhibited state must have JH/JH interface disrupted to sterically match HRSL with the inactive dimer of GCN2 kinase (Fig. 4C) and to account for the deleterious effect of the L1007A and V1021N mutations (Fig. 5). GCN2 becomes activated once it encounters translationally compromised ribosomes. These ribosomes likely outcompete (distract) the auto-inhibiting domains of GCN2, allowing stored free energy in separated JH helices to be released via JH/JH dimerization. The resulting JH/JH dimerization switches GCN2 kinase from the inactive kinase dimer to the active dimer (Figs. 4C, D and 6, last panel). We predict that the main HRSL domain remains constitutively dimeric in both active and inactive states of GCN2. This prediction is based on constitutive dimeric state of known tRNA synthetases and on our experimental observation that HRSL remains dimeric even when the dimerizing JH helices are truncated (Figs. 2E and S2). Multiple sequence alignment shows that linker between kinase and HRSL domain is a conserved element of GCN2, suggesting that our model likely applies to all GCN2 proteins from yeasts to human (Fig. S6).

Database depositions

Coordinates and cryo-EM map were deposited to the PDB and EMDB databases under accession numbers PDB ID 9BF3 and EMD-44489.

Note added in revision

After our work was completed and manuscript was finished (37), a related work was published by Yin et al. (27). and Bou-Nader et al. (38). References and discussion of the competing work were included during revisions.

Materials and methods

Kluyveromyces marxianus GCN2 HRSL sequence (Table S2) was inserted into pETM11-SUMO vector and expressed in *Escherichia coli* and purified to homogeneity by size exclusion fast protein liquid chromatography (FPLC). Cryo-EM samples were prepared with Quantifoil 1.2/1.3 on Cu 300 mesh holey carbon film using FEI vitrification robot. Cryo-EM data were collected using a Titan Krios G3 cryo-transmission electron microscope at 300 kV. Data processing was done with cryoSPARC v4.4.1 (39) (for the 3.2 Å structure) and RELION (40) (for the 6 Å dataset). AlphaFold prediction of initial model of GCN2 HRSL was obtained using a local installation of AlphaFold (25). The model was real-space refined in Phenix and Coot (41–43). In vitro kinase assays were conducted at 32 °C using eIF2α from LifeSpan Biosciences. *K. marxianus* kinase/HRSL domain sequence (Table S2) was inserted into pcDNA4.TO and expressed in HEK293T cells. Cells were grown in DMEM media + 10% FBS (Gibco). eIF2α phosphorylation was measured via western blot using primary antibodies for eIF2α phospho-S51 (Abcam) and total eIF2α (Cell Signaling Technologies). Detailed materials and methods are provided in SI.

Acknowledgments

We thank Prof. Frederick Hughson and Dr. Sarah Port for providing genomic DNA for *K. marxianus* and for sharing purified SUMO-protease. We are grateful for Prof. Yibin Kang Laboratory for providing HEK293T cells. We would like to acknowledge Princeton's Imaging and Analysis Center (IAC), which is partially supported through the Princeton Center for Complex Materials, and by National Science Foundation -MRSEC program (DMR-2011750). We thank Dr. Paul Shao and staff from IAC for their expertise and assistance with cryo-EM data collection. We thank Dr. Matthew Cahn from Princeton University Research Computing for cryo-EM computational support. Molecular graphics and analyses performed with UCSF Chimera were developed by the Resource for Biocomputing, Visualization, and Informatics at the University of California, San Francisco, with support from NIH P41-GM103311.

Supplementary Material

Supplementary material is available at *PNAS Nexus* online.

Funding

This study was funded by NIH grant 1R01GM110161-01 (to A.K.), Sidney Kimmel Foundation grant AWD1004002 (to A.K.), Burroughs Wellcome Fund grant 1013579 (to A.K.), and The Vallee Foundation (A.K.) and by NIGMS training grant 5T32GM007388 (to K.S.). X.F. was supported by the HFSP Long-Term Fellowship (LT000754) from the International Human Frontier Science Program Organization. G.D. and A.A.K. were funded by R35 GM127094.

Author Contributions

K.S.-K. performed cloning, purification, electron microscopy data collection, 6.1 Å data processing for ΔN GCN2 HRSL, initial data processing for WT GCN2 HRSL, and biochemical analyses. X.F. and N.Y. guided electron microscopy sample preparation, electron microscopy data collection, and data processing. D.G. and A.A.K. generated AlphaFold model of GCN2 HRSL from *K. marxianus* and performed 3.2 Å cryo-EM data processing and structure refinement. K.S.-K. and A.V.K. wrote the manuscript. All authors revised the manuscript, and K.S.-K., A.A.K., and A.K. finalized the manuscript.

Preprints

This manuscript was posted on a preprint: [DOI: https://doi.org/10.1101/2024.04.24.591037].

Data Availability

All materials used in this work are available from commercial sources: K.S.-K., X.F., D.G., A.A.K., N.Y., and A.K., Cryo-EM structure of GCN2 HRSL domain, PDB database: https://www.rcsb.org, accession number 9BF3, 2024; Cryo-EM Map; EMDB databases, https://www.emdataresource.org, accession number EMD-44489, 2024.

References

1 Sattlegger E, Hinnebusch AG. 2000. Separate domains in GCN1 for binding protein kinase GCN2 and ribosomes are required for GCN2 activation in amino acid-starved cells. *EMBO J*. 19: 6622–6633.
2 Costa-Mattioli M, Walter P. 2020. The integrated stress response: from mechanism to disease. *Science*. 368:eaat5314.
3 Taniuchi S, Miyake M, Tsugawa K, Oyadomari M, Oyadomari S. 2016. Integrated stress response of vertebrates is regulated by four eIF2alpha kinases. *Sci Rep*. 6:32886.
4 Ricketts MD, Emptage RP, Blobel GA, Marmorstein R. 2022. The heme-regulated inhibitor kinase requires dimerization for heme-sensing activity. *J Biol Chem*. 298:102451.
5 Carrara M, Prischi F, Nowak PR, Ali MM. 2015. Crystal structures reveal transient PERK luminal domain tetramerization in endoplasmic reticulum stress signaling. *EMBO J*. 34:1589–1600.
6 Dey M, Mann BR, Anshu A, Mannan MA. 2014. Activation of protein kinase PKR requires dimerization-induced cis-phosphorylation within the activation loop. *J Biol Chem*. 289: 5747–5757.
7 Dar AC, Dever TE, Sicheri F. 2005. Higher-order substrate recognition of eIF2alpha by the RNA-dependent protein kinase PKR. *Cell*. 122:887–900.
8 Anthony TG, *et al*. 2004. Preservation of liver protein synthesis during dietary leucine deprivation occurs at the expense of skeletal muscle mass in mice deleted for eIF2 kinase GCN2. *J Biol Chem*. 279:36553–36561.
9 Guo F, Cavener DR. 2007. The GCN2 eIF2alpha kinase regulates fatty-acid homeostasis in the liver during deprivation of an essential amino acid. *Cell Metab*. 5:103–114.

10 Tsai JC, *et al.* 2018. Structure of the nucleotide exchange factor eIF2B reveals mechanism of memory-enhancing molecule. *Science*. 359:eaaq0939.

11 Costa-Mattioli M, *et al.* 2005. Translational control of hippocampal synaptic plasticity and memory by the eIF2alpha kinase GCN2. *Nature*. 436:1166–1173.

12 Cui W, Li J, Ron D, Sha B. 2011. The structure of the PERK kinase domain suggests the mechanism for its activation. *Acta Crystallogr D Biol Crystallogr*. 67:423–428.

13 Wang P, Li J, Tao J, Sha B. 2018. The luminal domain of the ER stress sensor protein PERK binds misfolded proteins and thereby triggers PERK oligomerization. *J Biol Chem*. 293:4110–4121.

14 Nanduri S, Carpick BW, Yang Y, Williams BR, Qin J. 1998. Structure of the double-stranded RNA-binding domain of the protein kinase PKR reveals the molecular basis of its dsRNA-mediated activation. *EMBO J*. 17:5458–5465.

15 Nameki N, *et al.* 2004. Solution structure of the RWD domain of the mouse GCN2 protein. *Protein Sci*. 13:2089–2100.

16 Garcia-Barrio M, Dong J, Ufano S, Hinnebusch AG. 2000. Association of GCN1-GCN20 regulatory complex with the N-terminus of eIF2alpha kinase GCN2 is required for GCN2 activation. *EMBO J*. 19:1887–1899.

17 Hei Z, *et al.* 2021. Crystal structures reveal a novel dimer of the RWD domain of human general control nonderepressible 2. *Biochem Biophys Res Commun*. 549:164–170.

18 He H, *et al.* 2014. Crystal structures of GCN2 protein kinase C-terminal domains suggest regulatory differences in yeast and mammals. *J Biol Chem*. 289:15023–15034.

19 Lageix S, Zhang J, Rothenburg S, Hinnebusch AG. 2015. Interaction between the tRNA-binding and C-terminal domains of yeast Gcn2 regulates kinase activity in vivo. *PLoS Genet*. 11: e1004991.

20 Padyana AK, Qiu H, Roll-Mecak A, Hinnebusch AG, Burley SK. 2005. Structural basis for autoinhibition and mutational activation of eukaryotic initiation factor 2alpha protein kinase GCN2. *J Biol Chem*. 280:29289–29299.

21 Fujimoto J, *et al.* 2019. Identification of novel, potent, and orally available GCN2 inhibitors with type I half binding mode. *ACS Med Chem Lett* 10:1498–1503

22 Maia de Oliveira T, *et al.* 2020. The structure of human GCN2 reveals a parallel, back-to-back kinase dimer with a plastic DFG activation loop motif. *Biochem J*. 477:275–284.

23 Lageix S, Rothenburg S, Dever TE, Hinnebusch AG. 2014. Enhanced interaction between pseudokinase and kinase domains in Gcn2 stimulates eIF2α phosphorylation in starved cells. *PLoS Genet*. 10:e1004326.

24 Endicott JA, Noble ME, Johnson LN. 2012. The structural basis for control of eukaryotic protein kinases. *Annu Rev Biochem*. 81: 587–613.

25 Jumper J, *et al.* 2021. Highly accurate protein structure prediction with AlphaFold. *Nature*. 596:583–589.

26 Tian Q, Wang C, Liu Y, Xie W. 2015. Structural basis for recognition of G-1-containing tRNA by histidyl-tRNA synthetase. *Nucleic Acids Res*. 43:2980–2990.

27 Yin JZ, *et al.* 2024. The HisRS-like domain of GCN2 is a pseudoenzyme that can bind uncharged tRNA. *Structure*. 32:795–811.e796.

28 Dong J, Qiu H, Garcia-Barrio M, Anderson J, Hinnebusch AG. 2000. Uncharged tRNA activates GCN2 by displacing the protein kinase moiety from a bipartite tRNA-binding domain. *Mol Cell*. 6: 269–279.

29 Inglis AJ, *et al.* 2019. Activation of GCN2 by the ribosomal P-stalk. *Proc Natl Acad Sci U S A*. 116:4946–4954.

30 Harding HP, *et al.* 2019. The ribosomal P-stalk couples amino acid starvation to GCN2 activation in mammalian cells. *Elife*. 8: e50419.

31 Jiménez-Díaz A, Remacha M, Ballesta JP, Berlanga JJ. 2013. Phosphorylation of initiation factor eIF2 in response to stress conditions is mediated by acidic ribosomal P1/P2 proteins in *Saccharomyces cerevisiae*. *PLoS One*. 8:e84219.

32 Inglis AJ. 2018. Structural and functional characterisation of the nutrient sensing kinase GCN2. Downing College PhD Thesis.

33 Kane SM, Vugrincic C, Finbloom DS, Smith DW. 1978. Purification and some properties of the histidyl-tRNA synthetase from the cytosol of rabbit reticulocytes. *Biochemistry*. 17:1509–1514.

34 Wu CC, Peterson A, Zinshteyn B, Regot S, Green R. 2020. Ribosome collisions trigger general stress responses to regulate cell fate. *Cell*. 182:404–416.e414.

35 Yan LL, Zaher HS. 2021. Ribosome quality control antagonizes the activation of the integrated stress response on colliding ribosomes. *Mol Cell*. 81:614–628.e614.

36 Gupta R, Hinnebusch AG. 2023. Differential requirements for P stalk components in activating yeast protein kinase Gcn2 by stalled ribosomes during stress. *Proc Natl Acad Sci U S A*. 120: e2300521120.

37 Solorio-Kirpichyan K, *et al.* 2024. Cryo-EM structure of HRSL domain reveals activating crossed helices at the core of GCN2. BioRxiv 591037. https://doi.org/10.1101/2024.04.24.591037, preprint: not peer reviewed

38 Bou-Nader C, *et al.* 2024. Gcn2 structurally mimics and functionally repurposes the HisRS enzyme for the integrated stress response. *Proc Natl Acad Sci U S A*. 121:e2409628121.

39 Punjani A, Rubinstein JL, Fleet DJ, Brubaker MA. 2017. Brubaker, cryoSPARC: algorithms for rapid unsupervised cryo-EM structure determination. *Nat Methods*. 14:290–296.

40 Scheres SHW. 2012. RELION: implementation of a Bayesian approach to cryo-EM structure determination. *J Struct Biol*. 180: 519–530.

41 Adams PD, *et al.* 2002. PHENIX: building new software for automated crystallographic structure determination. *Acta Crystallogr D Biol Crystallogr*. 58:1948–1954.

42 Liebschner D, *et al.* 2019. Macromolecular structure determination using X-rays, neutrons and electrons: recent developments in Phenix. *Acta Crystallogr D Struct Biol*. 75:861–877.

43 Afonine PV, *et al.* 2018. Real-space refinement in PHENIX for cryo-EM and crystallography. *Acta Crystallogr D Struct Biol*. 74: 531–544.